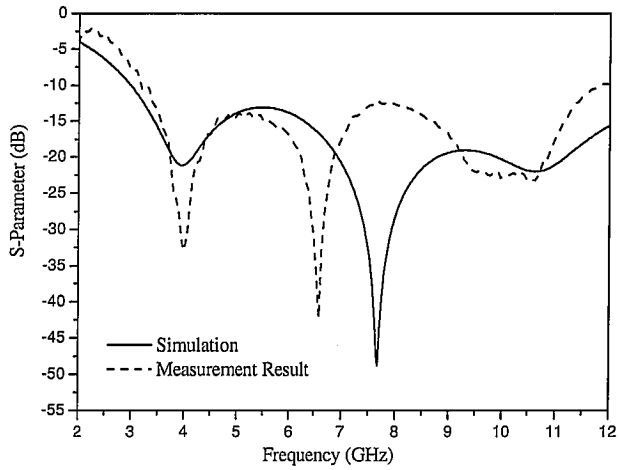

Figure 12 Measured and simulated return loss of the antenna

and measured results are displayed. A good agreement between simulated and measured S-parameter has been obtained. Although the spectrum of the emitted pulse is in 3–5 GHz, potentially, the proposed antenna can be used for full UWB frequency band in the future research.

5. CONCLUSION

A fully integrated CMOS UWB transmitter is presented. The transmitter consists of a UWB antenna and a transmitter IC which integrates a pulse generator, a pulse modulator, and a DA. A novel all-digital low-power UWB pulse generator and pulse modulator are proposed. A DA is employed after pulse modulation to shape the pulse such that its frequency spectrum fits the FCC spectral mask and to drive the antenna. The transmitter chip has been demonstrated in a 0.18-μm CMOS technology.

REFERENCES

1. FCC notice of proposed rule making, revision of part 15 of the commission's rules regarding ultra-wideband transmission systems, FCC, Washington, DC, ET-docket 98–153.
2. Y. Jeong, S. Jung, and J. Liu, A CMOS impulse generator for UWB wireless communication systems, IEEE ISCAS 4 (2004), 129–132.
3. P.K. Saha, N. Sasaki, and T. Kikkawa, A CMOS UWB transmitter for intra/inter-chip wireless communication, Int Symp Spread Spectrum Tech Appl (2004), 962–966.
4. J. Ryckaert, et al., Ultra-wide-band transmitter for low-power wireless body area networks: Design and evaluation, IEEE Trans Circ Syst 52 (2005), 2515–2525.
5. H. Kim and Y. Joo, Fifth-derivative Gaussian pulse generator for UWB system, IEEE Radio Frequency Integrated Circuits Symposium, Long Beach, CA, June 12–14, 2005, pp. 671–674.
6. T. Norimatsu, et al., A novel UWB impulse-radio transmitter with all-digitally-controlled pulse generator, Eur Solid State Circ Conf (2005), pp. 267–270.
7. A. Bevilacqua and A.M. Niknejad, An ultra-wideband CMOS low-noise amplifier for 3.1-10.6GHz wireless receivers, IEEE J Solid State Circ 39 (2004), pp. 2259–2268.

AIR-BRIDGE-INTEGRATED STUB FILTER FOR SUBMILLIMETER WAVE APPLICATIONS

Dazhen Gu,[1] Fernando Rodriguez-Morales,[2] and Sigfrid K. Yngvesson[3]
[1] National Institute of Standards and Technology, Electromagnetics Division, 325 Broadway, Boulder, CO 80305; Corresponding author: dazhen.gu@boulder.nist.gov
[2] Center for Remote Sensing of Ice Sheets, 2335 Irving Hill Rd, Lawrence, KS 66045
[3] Department of Electrical and Computer Engineering, University of Massachusetts, Amherst, MA 01003

Received 22 September 2008

ABSTRACT: *We report a coplanar waveguide notch filter with an integrated air-bridge, designed for operation at submillimeter wave frequencies and cryogenic temperatures. The filter is built with a planar slot-ring antenna, which is in turn loaded with a superconducting mixer detector. The filter is designed to have a narrow-band response with 40 dB of attenuation at 1.56 THz. The fabrication of the micrometer-scale structure was accomplished by means of UV photolithography and electroplating. The optimized microelectronic fabrication process produced high yields and good reliability. Preliminary measurements of a submillimeter wave receiver based on this design showed satisfactory performance of the filter.* © 2009 Wiley Periodicals, Inc. Microwave Opt Technol Lett 51: 1436–1439, 2009. *This article is a US Government work and, as such, is in the public domain in the United States of America. Published online in Wiley InterScience (www.interscience.wiley.com). DOI 10.1002/mop.24375

Key words: *air-bridge; band-stop filter; electroplating; microfabrication; submillimeter wave systems*

1. INTRODUCTION

The submillimeter (sub-mm) wave region of the electromagnetic spectrum corresponds to the span of wavelengths from 100 μm to 1 mm (or equivalently frequencies ranging from 300 GHz to 3 THz). Distinct properties of sub-mm waves as well as unique signatures of various materials in this frequency range have stimulated considerable research interests in this field for the past twenty years. Applications in this frequency band evolved from the early radio astronomy to recent plasma diagnostics [1], security, and biomedical imaging [2, 3], as well as genetic sequence identification [4]. All these applications benefit from the developments of reliable and miniaturized sub-mm wave systems and components.

In this article, we present the design and fabrication of an air-bridge-integrated coplanar waveguide (CPW) stub filter with narrow band-stop response that is designed to function in conjunction with a mixer-loaded monolithic antenna. This structure constitutes the frontend of a generic sub-mm wave heterodyne receiver, which we characterized in terms of its sensitivity. Although the air-bridge technique has been widely used for applications at much lower frequencies [5, 6], the integration of air-bridges with sub-mm wave components present significant challenges, especially on fabrication, which will be addressed in this article.

2. DESIGN DESCRIPTION

The monolithic structure we report is intended for operation at 1.56 THz, corresponding to a free-space wavelength of 192.3 μm. The choice of the operating frequency is a consideration for ground-based applications since 1.56 THz falls within one of the well known frequency windows with low atmospheric attenuation. A slot-ring antenna was chosen to quasi-optically couple the local

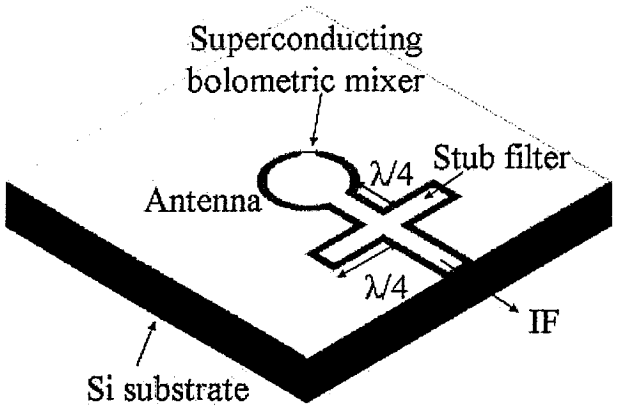

Figure 1 Illustration of the monolithic structure. The stub filter is integrated with a superconducting mixer-loaded antenna. λ/4 corresponds to one quarter of the guided wavelength at the frequency of operation (19 μm for 1.56 THz when a Si substrate is used). [Color figure can be viewed in the online issue, which is available at www.interscience.wiley.com]

oscillator (LO) and radio-frequency (RF) signal beams into a heterodyne detector, as shown in Figure 1 [7]. The superconducting detector (4 μm wide and 1 μm long) is based on a 3 nm thick NbN film and was operated in a bolometric mixing mode. The down-converted intermediate frequency (IF) output signal of the antenna/mixer combination was coupled to the external circuitry by means of a CPW transmission line.

The proposed notch filter is required immediately after the radiating structure in order to block any leakage from the LO and RF signals into the IF signal path. A double-stub filtering structure presents a very high impedance (equivalent to an open circuit) to the interface between the antenna and the external circuitry, thus producing high rejection at the frequency of interest. This configuration is preferred over other common alternatives (such as stepped impedance filters), particularly when narrow bandwidths are required and when space is limited, as, for example, in array applications. In addition, stub structures in filter design are simple to analyze. Stub filters implemented in CPW technology, however, create discontinuities in the transmission line structure, which result in the propagation of high-order slot-line modes and hence degrade the filter performance. Undesired high-order modes reduce the sensitivity of the receiver by introducing extra losses in the RF and LO signal paths to the active device. To circumvent the problems mentioned above, an air-bridge structure is needed to even the ground potential in the proximity of the discontinuities and properly direct the ground currents.

The CPW lines for the filter were fabricated on a square silicon substrate (6 mm by 6 mm). The width of the inner conductor is 3.6 μm, whereas the slot width is 2 μm. This results in a characteristic impedance of ~50 Ω when the silicon substrate is used. The filter consists of two quarter-wave (19 μm) open-circuit stubs located one quarter of a wavelength away from the antenna.

3. COMPUTER SIMULATIONS

We first performed full-wave electromagnetic (EM) simulations on the proposed filter structure in the absence of an air-bridge. The ground plane was locally divided by the stub filters and the CPW into four quadrants. With this arrangement, the discontinuities of the CPW excited the unwanted slot-line modes, as shown in Figure 2(a) and facilitated the propagation of the LO and RF signals through the filter. As expected, the filter without an air-bridge structure exhibited no band-stop filtering behavior, as shown in Figure 3 (black dotted curves).

Next, an air-bridge structure was incorporated into the filter in order to achieve the desired narrow-band operation. According to the simulations, the addition of the air-bridge clearly improves the filter performance by effectively suppressing slot-line modes [Fig. 2(b)]. The preliminary design, however, presented a resonance centered at a much higher frequency (1.85 THz) than the desired 1.56 THz, as shown in Figure 3 (blue dashed curves).

The shift of the resonance can be explained as follows. On one hand, the air-bridge introduces parasitic capacitance, which tends to lower the resonant frequency. The predicted parasitic capacitance of air-bridges at terahertz frequencies is estimated from the parallel-plate approximation, having a negligible value in the order of 10^{-5} pF. On the other hand, the effective dielectric constant is reduced in the air-bridge area, resulting in an increase of the resonant frequency [8]. The simulation data confirm that the reduction of the effective dielectric constant dominates the resonance shift in our air-bridge structure.

We then used the optimization tools in the EM simulator to compensate for the shift in the filter response to find the best geometry that would yield an insertion loss (S_{21}) greater than 30 dB at 1.56 THz. The parameter adjusted during the optimization process was primarily the length of the stub. The layout of the optimized design is shown in Figure 4, which produced about 40 dB of insertion loss at 1.56 THz in the software environment. The

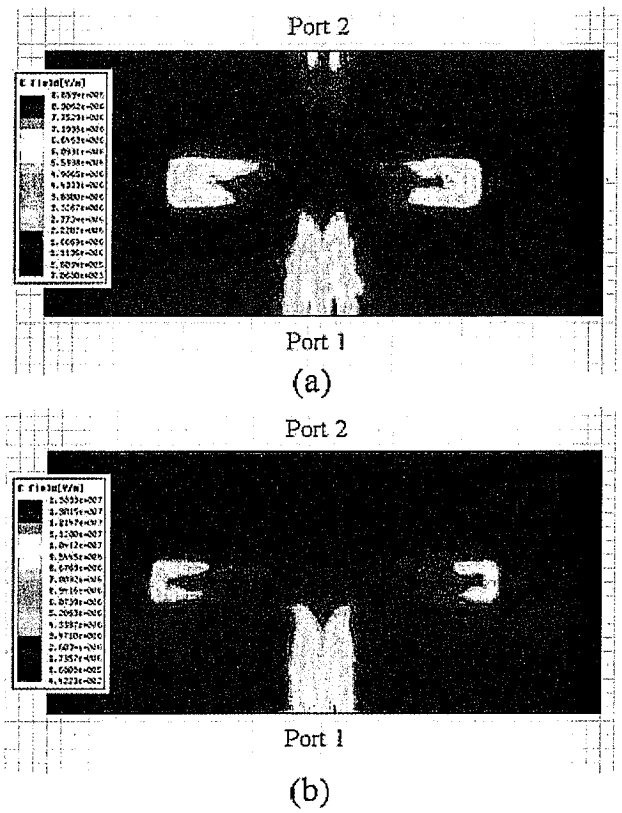

Figure 2 Simulated electric field distribution in the filter structure for different configurations: (a) Stub filter without air-bridges, where slot-line modes will carry the energy flow from Port 1 to Port 2 and; (b) Stub filter with an air-bridge incorporated, where suppression of slot-line modes ensures adequate filter response. [Color figure can be viewed in the online issue, which is available at www.interscience.wiley.com]

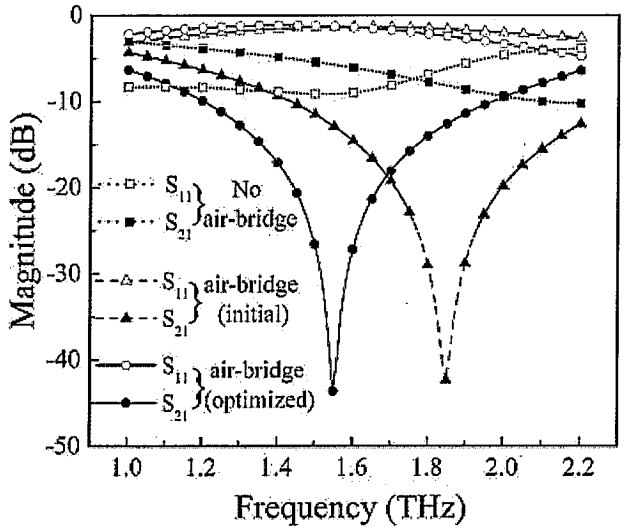

Figure 3 Scattering parameters obtained from EM simulations for different filter layouts: (1) filter without air-bridges; (2) initial filter design with air-bridges; and (3) final optimized design. [Color figure can be viewed in the online issue, which is available at www.interscience.wiley.com]

predicted 20-dB bandwidth of the optimized filter was about 150 GHz.

4. FABRICATION OF AIR-BRIDGE-INTEGRATED FILTER

All the planar components, including the mixer, the antenna, and the filter, were fabricated on a high-purity silicon substrate by means of UV photo-lithography. A projection printer was used as the main lithographic instrument with a resolution of 0.5 μm and overlay accuracy better than 0.1 μm. Two primary marks were patterned on the substrate before the device fabrication. These marks were used as the alignment reference for the entire fabrication process, including the following steps of air-bridge construction.

The micromachined air-bridge was fabricated on top of the planar components. The steps involved in the fabrication procedure are outlined in Figure 5. Two main steps were building four posts on the ground plane and then connecting them with a frame. The posts were 6 μm tall and the frame was 3 μm thick, which both were constructed by a gold electroplating process. The gold plating step was carried out by the use of a commercially available noncyanide electrolytic solution at a temperature of 60°C. The thickness of the electroplated gold was controlled by the plating time, with the current density fixed at 2 mA/cm^2. The resulting electroplating rate was 0.11 μm/min. The electroplating process was completed using a commercial plating bath. Plating cell configurations utilized a rotating wheel (cathode), where one wafer can be attached, along with reciprocating anodes. The plating system produced a uniform coating and a constant deposition rate. During plating, as the wafer rotated, the anodes moved continuously from one side to the other, whereas a high precision pulsed DC power supply regulated the voltage in order to maintain a constant deposition rate.

Different types of photoresists were used as sacrificial layers to accommodate different thicknesses of gold for the posts and the frame. To form a 6 μm thick sacrificial layer for realizing the standing posts, a thick photoresist was coated and patterned by means of projection printing. The patterned sacrificial layer was thermally cured at 115°C in order to harden the photoresist for the following gold post growth in the electroplating bath. After the electroplating step, a titanium-gold layer was coated onto the entire substrate by E-beam evaporation while leaving the primary marks uncovered for the following alignment purpose. This titanium-gold layer provides electro-contact for the following gold plating step. Next, an additional thick photoresist layer was spun on and patterned to form a 3 μm thick sacrificial layer. After the photoresist was cured, a plating procedure was repeated to form 3 μm thick

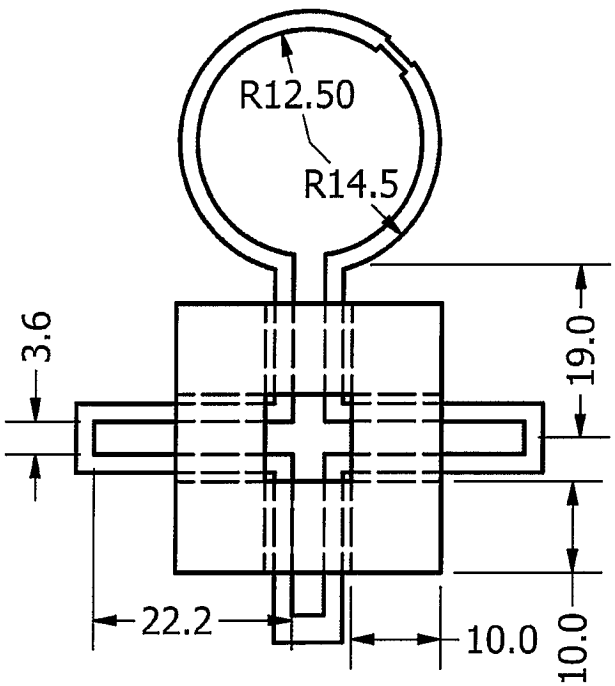

Figure 4 Final layout of the air-bridge-integrated stub filter (units are μm)

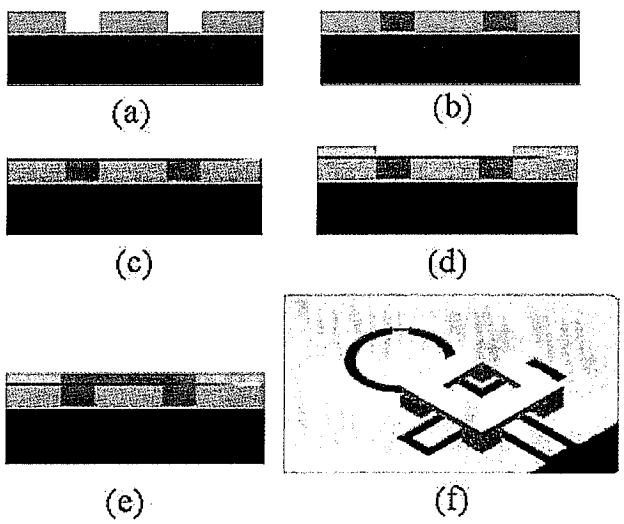

Figure 5 Air-bridge fabrication steps: (a) pattern first layer photoresistor for building posts; (b) gold-plating 6 μm thick posts; (c) coat Ti-Au contact layer; (d) pattern second layer photo-resistor for building spans; (e) gold-plating 3 μm thick spans; (f) lift-off unwanted metal and remove sacrificial layers. [Color figure can be viewed in the online issue, which is available at www.interscience.wiley.com]

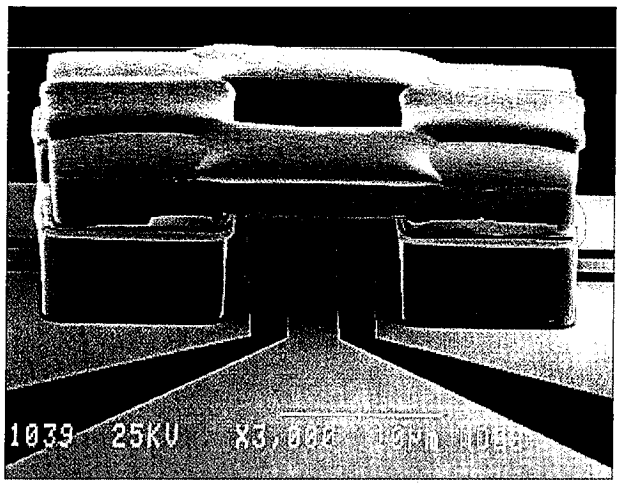

Figure 6 SEM photograph of a fabricated sample air-bridge structure

gold. Finally, the substrate was immersed in a photoresist remover solvent kept in a warm water bath in order to strip off the sacrificial layer and the excess metal. Ultra-sound agitation may be used to accelerate the lift-off step.

The novelty of this fabrication process lies in the use of UV photolithography. The micromachining of three-dimensional structures at such a small scale is very often implemented by more sophisticated E-beam lithographic techniques. In addition, no thermal stresses are introduced during the removal of the sacrificial layers, when compared with other techniques, such as oxygen ash. As a result, the air-bridges made in our process are less prone to bend or bow, which often occurs in plasma ash techniques [9]. Furthermore, solvent strip does not deteriorate active devices, such as the superconducting mixers used in this work. The fabrication process was optimized to achieve a high yield: 95% on the wafer and 75% on the small chip.

Figure 6 shows a scanning electron microscope (SEM) image of one of the fabricated air-bridges. The dimensions of the air-bridge agree well with the design specification.

5. EXPERIMENTAL RESULTS

The DC resistance between divided ground planes was measured to be less than 5 Ω, indicating a good contact between the ground planes and the air-bridges. Furthermore, nearly all the air-bridges fabricated survived ultrasound agitation as well as the cryogenic temperature cycling. Because most sub-mm wave receiver front-ends are operated in a cryogenic environment, mechanical strength and endurance to thermal stress of the fabricated structures are one of the crucial design considerations for most sub-mm wave components.

Direct and accurate assessment of the performance of the manufactured filter would require calibrated tunable sources at these extremely high frequencies, which are not available in presence. To validate the effectiveness of our fabrication approach, we measured the receiver sensitivity of a sample structure, and compared it with that of a similar device where no air-bridge was incorporated. We followed a conventional Y-factor approach to measure the receiver sensitivity [3]. We found that the receivers with air-bridge integration did not produce higher sensitivity than those without air-bridges. From previous experiences [3], we noted that the quality of the mixer predominates the sensitivity of the sub-mm receiver. Therefore, further experiments are required to justify the necessity of the air-bridge integration in the future. The device with the integrated air-bridge, however, required an LO drive level much lower than that for its counterpart. This gives an indication of lower LO leakage through the IF port when the air-bridge is present.

6. CONCLUSIONS

An air-bridge-integrated double-stub filter with narrow stop-band response has been demonstrated in CPW technology for sub-mm wave applications. Computer simulations showed an insertion loss of about 40 dB at 1.56 THz. The fabrication of planar filter structures and air-bridges was successfully implemented by UV lithography and electroplating. The air-bridges showed good mechanical stability, suitable for functioning at low temperatures. Although characterization of the air-bridge-integrated filter is limited at the present, preliminary measurements showed a low LO power consumption for the devices with air-bridge integration, which is a critical design consideration due to the limited power budget in the sub-mm regime. The novel fabrication technique presented in this article offers an effective method for making highly integrated three-dimensional microelectronic structures operating in the sub-mm wave regime and/or cryogenic environment.

ACKNOWLEDGMENTS

We thank Dr. E. Gerecht and Dr. J. Moreland for valuable discussions. The authors are also grateful to Mr. Xin Xhao for his help in measuring some of the fabricated structures.

REFERENCES

1. D.L. Brewer, K.W. Kim, L. Zeng, Y. Jiang, E. Doyle, and W.A. Peebles, Integrated reflectometer-interferometer system for plasma density profile measurement, Plasma Phys Controlled Fusion 40 (1998), 1575–1584.
2. J.F. Federici, B. Schulkin, F. Huang, D. Gary, R. Barat, F. Oliveira, and D. Zimdars, THz imaging and sensing for security applications-explosives, weapons and drugs, Semicond Sci Technol 20 (2005), S266–S280.
3. F. Rodriguez-Morales, S. Yngvesson, R. Zannoni, E. Gerecht, D. Gu, N. Wadefalk, and J. Nicholson, Development of integrated HEB/MMIC receivers for near-range terahertz imaging, IEEE Trans Microwave Theory Tech 54 (2006), 2301–2311.
4. M. Nagel, F. Richter, P. Haring-Bolivar, and H. Kurz, A functionalized THz sensor for marker-free DNA analysis, Phys Med Biol 48 (2003), 3625–3636.
5. P. Sewell and T. Rozzi, Characterization of air-birdges in mm-wave coplanar waveguide using the complete mode spectrum of CPW, IEEE Trans Microwave Theory Tech 42 (1994), 2078–2086.
6. J. Lee, H. Lee, W. Kim, J. Lee, and J. Kim, Suppression of coupled-slotline mode on CPW using air-bridges measured by picosecond photoconductive sampling, IEEE Microwave Guided Wave Lett 9 (1999), 265–267.
7. S.K. Masarweh, T.N. Sherer, K.S. Yngvesson, R.L. Gingras, C. Drubin, A.G. Cardiasmenos, and J. Wolverton, Modeling of a monolithic slot ring quasi-optical mixer, IEEE Trans Microwave Theory Tech 42 (1994), 1602–1609.
8. N.H.I. Koster, S. Koblowski, R. Bertenburg, S. Heinen, and I. Wolff, Investigation on air-bridges used for MMIC's in CPW technique, Proc Eur Microwave Conf (1989), 666–671.
9. M.A. Gritz, J. Gonzalez, and G.D. Boreman, Fabrication of infrared antennas using electron beam lithography, Proc SPIE 4984 (2003), 100–110.